SIMULATION OF CREEP CRACK GROWTH OF A DIRECTIONALLY-SOLIDIFIED NI-BASE SUPERALLOY

Ali P. Gordon[1], Mahesh M. Shenoy[1], David L. McDowell[12]
[1]George W. Woodruff School of Mechanical Engineering, Atlanta, GA 30332-0405
[2]School of Materials Science and Engineering, Atlanta, GA 30332-0245

ABSTRACT

Creep lifetime of turbine blade material subjected to sustained centrifugal forces at elevated temperatures is limited by accumulated inelastic deformation and creep crack growth (CCG). Creep resistance exhibited in conventionally cast polycrystalline (PC) Ni-base superalloy components has been enhanced via solidification techniques. Directional solidification (DS) results in large grain sizes with limited misorientation at grain boundaries. The present study focuses on a Ni-base superalloy in DS form at 871ºC. Data obtained from deformation experiments performed on longitudinal (L) and transverse (T) specimens are used to develop an anisotropic elasto-creep material model. Simulated time-dependent, asymptotic crack tip fields of compact tension (CT) specimens are applied in the calculation of creep zones and fracture parameters, and are discussed in relation to crack growth rate. The microstructure of each CT model differs in terms of grain orientation (i.e., L-T or T-L), crack behavior (i.e., stationary or growing), and other graain attributes. Since each model is subjected to identical loading conditions, effects of microstructural configurations on inelastic deformation are emphasized.

1 INTRODUCTION

Although some studies have considered CCG behavior of DS Ni-base superalloys, the vast majority have focused on materials with PC microstructures. Each sought to improve life prediction techniques for power generation components by way of correlating CCG rates with fracture mechanics parameters, such as the Mode I stress intensity factor K_I or the C^*-integral. To this endeavor, many investigators subjected CT specimens to a variety of testing configurations. Afterwards, additional information was gathered from the fracture surfaces using scanning electron microscopy (SEM) to determine the propagation mechanism and the crack growth type (Stage I or II). Depending on the test configuration (i.e., temperature, load amplitude, and rate) crack tip conditions can range from creep-brittle to creep-ductile. In the current investigation, we characterize the CCG behavior of DS Ni-base superalloys by parametrically studying the effect of varying the microstructural arrangement of the grains. These anisotropic crack tip fields are necessary for the development of HRR-type relations that characterize the appropriate fracture parameter(s).

Investigators have attempted to establish candidate fracture mechanics parameters as appropriate for the prediction of CCG rates in Ni-base superalloys; however because of the wide range of material variations (e.g. grain structure, chemical composition, inclusion content, casting porosity) and service conditions (e.g. temperature, mechanical load, environment), crack growth can occur by either creep-ductile or creep-brittle conditions. Under small-scale creep (SSC) conditions, Nazmy and Wuthrich [1] showed that CCG results of PC Ni-base superalloys can be curve-fit using a power law relations in terms of K_I. Above 800°C, SSC conditions are often violated, and K_I fails to predict CCG rates accurately. Both C_t and the C^*-integral have been investigated as viable fracture parameters since each is applicable during extensive creep (EC) [2, 3]. Although each parameter can be calculated in terms of load line deflection, these expressions were derived for homogeneous isotropic materials. For example, a measure of the creep deflection rate as stated in ASTM E1457 is

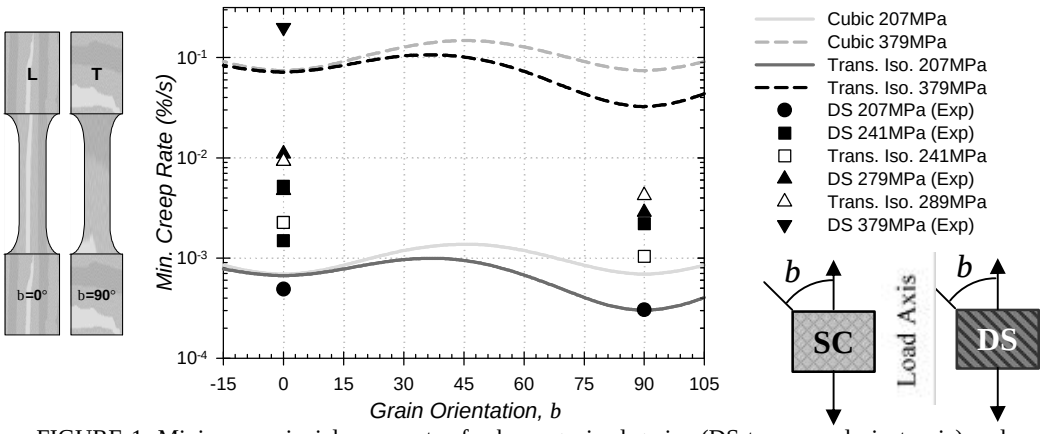

FIGURE 1: Minimum uniaxial creep rates for homogenized grains (DS-transversely isotropic) and single crystal (SC-cubic) materials using Hill's anisotropic yield function. Closed symbols represent experimental results.

$$\dot{d}_c = \dot{d} - \frac{\dot{a}B}{P}\left[\frac{2\left(1-n^2\right)K_I^2}{E}\right] \tag{1}$$

By Hoff's analogy, the C^*-integral was proposed as a parameter to correlate CCG rates [4, 5]:

$$C^* = \int_\Gamma \left(W^* dy - T_i \frac{\partial \dot{u}_i}{dx} ds \right) \tag{2}$$

where T_i is the traction vector and W^* is the strain rate energy density along the counter-clockwise contour G inside the crack tip region. Under EC conditions, for which creep strains dominate the remaining ligament, this expression can be valid along any contour, and is therefore path-independent. Under EC conditions, the C^*-integral completely characterizes the HRR fields in isotropic, power law creeping solids [6], i.e.,

$$s_{ij}(r,q) = \left[\frac{C^*}{AI_n r}\right]^{\frac{1}{n+1}} \hat{s}_{ij}(q,n) \quad ; \quad \dot{e}_{ij}(r,q) = A\left[\frac{C^*}{AI_n r}\right]^{\frac{n}{n+1}} \hat{e}_{ij}(q,n) \tag{3}$$

Here A and n are power law creep strain material constants and I_n is an integration constant. The last factors in each term are normalized self-similar functions which prescribe the field shape and are time-independent. The C_t-parameter is interchangeable with C^* in Eq. (3).

The availability of results from fracture modeling of Ni-base superalloys is very limited. Gardner and coworkers [2] modeled CT specimens with isotropic elastic and transversely isotropic creep properties. C^* was computed by approximating the material behavior of a DS alloy as transversely isotropic with time-dependent properties. The material was assumed to behave according to Norton's secondary power law such that A_T and A_L are the creep coefficients in the transverse and longitudinal orientations, respectively. Each were defined so that $5 \times A_T = A_L$.

2 MATERIAL AND EXPERIMENTS

Investment casting processes have been developed to enhance the creep strength of Ni-base superalloys beyond what can arguably be achieved by means of just altering the alloy chemistry. Depending on the manufacturing route, grains of Ni-base superalloys can range from several microns (PCs) to beyond several millimeters (single crystals-SCs) in size. Directional solidification creates columnar grains averaging 100*mm* long and between 0.5 and 4*mm* wide. This grain boundary (GB) structure improves the mechanical behavior of PC materials. For example, cavitation and sliding at grain interfaces are reduced. The long grains serve a fracture

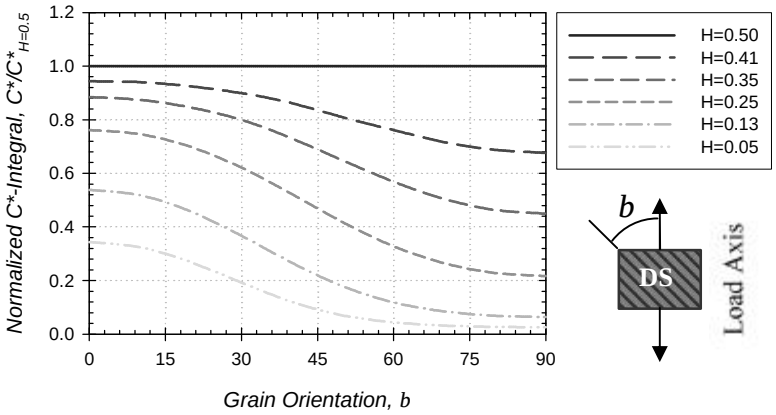

FIGURE 2: C^*-integral for DS material modeled as homogenized material under plane *s* conditions.

toughening mechanism since slow moving cracks are often deflected near GB interfaces.

Isothermal mechanical testing has been carried out on samples machined from a DS cast plate. Heat was supplied by a resistance furnace that permitted unforced circulation of lab air. Two types of high temperature tests were performed uniaxial creep rupture and CCG. Creep deformation tests were performed on longitudinal (L) and transverse (T) specimens according to ASTM E139. The machining convention for creep specimens is shown in Fig. 1. The CCG tests were conducted to measure time-dependent crack growth rates and load-line deflection. Each CT specimen had a width of 50.8*mm* and thickness of 12.7*mm*. The initial crack length to width ratio, *a/W*, was 0.5. After precracking the specimen according to the procedures specified in ASTM E1457, the specimens were side-grooved by 10% of the thickness to prevent out-of plane crack growth during high-temperature testing. The DC electric potential technique was employed for crack length monitoring. Tests of T-L and L-T specimens were completed at 871°C. At this temperature, the possible effects of oxidation are limited. In each case, a load of 10.2*kN* was applied so that K_I=42*MPaÖm*. In application, the L-T specimen structure corresponds to the cracks perpendicular to longitudinal grains near the trailing edge, while the T-L specimen simulates a crack at a blade tip in which the grain orientation and the crack propagation direction are parallel.

3 NUMERICAL SIMULATIONS

Simulations of CCG in a DS Ni-base superalloy have been carried out using two modeling approaches: (1) *homogenizing grains* and (2) *explicit grains*. The former approach smears the affect of grain orientation and structure found in DS materials, while the latter simulates misorientation and structure of several long SC grains. In each case, a constitutive model that prescribed the elastic and secondary creep behavior exhibited in experiments was utilized. Anisotropic creep behavior is implemented using Hill's anisotropic yield function to describe crack tip deformation in a generic material such as DS René80, i.e.,

$$\tilde{q}(s) = \sqrt{F(s_y - s_z)^2 + H(s_z - s_x)^2 + I(s_x - s_y)^2 + 2Lt_{yz}^2 + 2Mt_{zx}^2 + 2Nt_{xy}^2} \tag{4}$$

where the constants, *F*, *H*, *I*, *L*, *M*, and *N* are independent for fully orthotropic creeping solids.

For the behavior of *homogenized grains*, the responses along the longitudinal and transverse orientations are considered. Since DS materials can be assumed as isotropic in the plane transverse to the DS axis, only 5 elastic constants are needed. The following constants were obtained from experiments at 871ºC: E_x=72*GPa*, E_y=95*GPa*, n_{zx}=0.55, n_{xy}=0.41, and G_{xy}=89*GPa*. Because of limited material supply, uniaxial creep tests could only be performed in the transverse

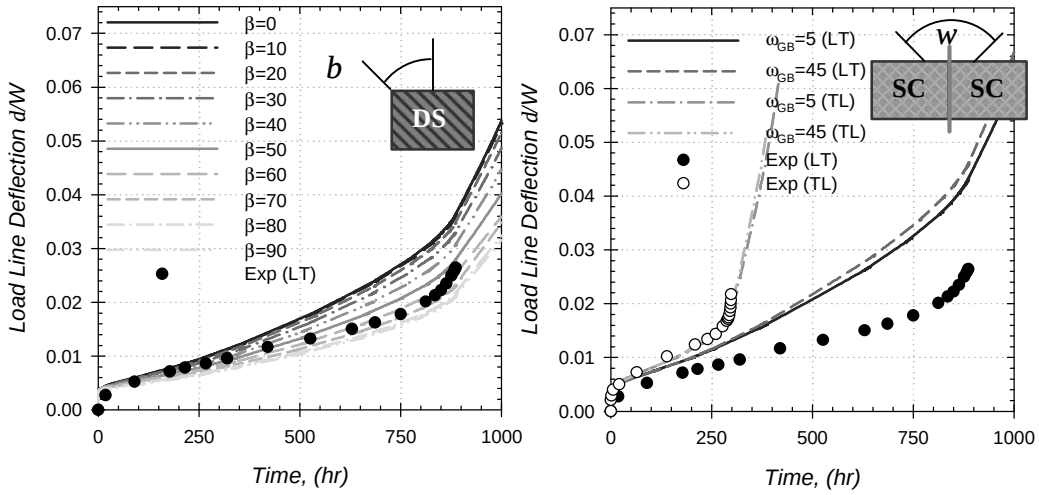

FIGURE 3: Plane stress load line deflection curves for DS material with the (left) homogenized response and (right) explicitly modeled long SC grains at 871°C and K_I=42*MPaÖm*.

(*x* and *z*) and longitudinal (*y*) axes. Using power law creep, stress for the uniaxial creep tests in the x_i-direction yields

$$\dot{e}_{cr}^{(x_i)} = A_{x_i}\left(s_{x_i}\right)^n = A\left(\tilde{q}\right)^n \tag{5}$$

where A_{x_i} and s_{x_i} is the steady-state creep coefficient and normal stress, respectively, in the x_i-direction. The relationships between the anisotropic creep coefficients and the equivalent creep coefficient are obtained by combining Eqs. (4) and (5). Without any loss of generality, if the DS and *y* axes are parallel, the mechanical properties are isotropic in the *xz*-plane. As a result, $A_x=A_z=A_T$. By setting $A=A_y=A_L$, the following equations are obtained

$$H = I = \frac{1}{2}\left(\frac{A_T}{A}\right)^{\frac{2}{n}} \quad , \quad F = \left(\frac{A_L}{A}\right)^{\frac{2}{n}} - H \tag{6}$$

Constants related to the shear stresses, *L*, *M*, and *N*, were identically set to unity. Data from uniaxial creep test results in the following creep properties: $A_x=A_T=3.1\times10^{-24} MPa^{-n}hr^{-1}$, $A_y=A_L=3.5\times10^{-21} MPa^{-n}hr^{-1}$, and n=7.7. It is important to note that the use of this approach allows for different creep coefficients to accommodate the material anisotropy, but the creep exponent is assumed to be identical in every direction. The constant *H* was set to 0.35 to minimize the error between experimental and simulated minimum creep rates shown in Fig. 1.

Explicitly simulating several adjacent SC grains requires that each grain be modeled as a cubic material. By convention, 3 elastic constants in cubic elastic constitutive equations are needed: *E*=95*GPa*, *n*=0.33, and *G*=89*GPa*. Since the creep response in the *x*, *y*, and *z*-directions are identical, *F*, *H*, and *I* must each be 0.5 according to Eq. (6). The creep rate in the [110] orientation is nearly twice that in the [100] orientation, as such, *L*, *M*, and *N* were optimized to 1.54. The minimum uniaxial creep rates for both the transversely isotropic and cubic materials loaded at different orientations relative to the axis of the crystal, *b*, are shown in Fig. 1. Behavior of the cubic material is *p/2* periodic, while that of the transversely isotropic material is *p*.

A finite element mesh simulating a full CT specimen consisting of two-dimensional (plane stress or plane strain) linear elements was used in the analyses. A portion of the elements were arranged in a uniform pattern along the crack plane to allow for incremental crack propagation via nodal release. To simulate experiments, load is applied at the center of the pinhole using a

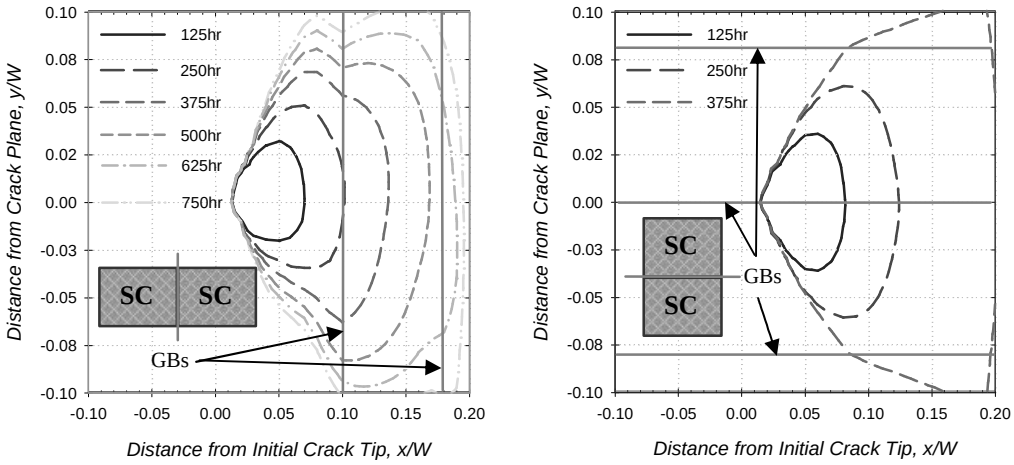

FIGURE 4: The effective 2% creep strain zones in (left) L-T and (right) T-L CT specimens subjected to CCG conditions at 42*MPaÖm* and 871ºC. Misorientation at long SC grain interfaces is w=45º.

specified dead-weight load facilitating K_I=*42MPaÖm*. Total crack length as a function of time was applied as the fracture criterion prescribing incremental crack propagation. Experimental and simulated load-line deflections are compared with numerical predictions in later sections. Stationary crack tip behavior was also considered to investigate the creep incubation behavior. The parameter that was varied for the *homogenized grains* is material (or grain) orientation with respect to the loading axis, b. As such, the b values over the range of *[0, p/2]* map to *[0, -p/2]*.

For *modeling of explicit SC grains*, the grain size, d_{GB}, and misorientation between adjacent SC grains in the *xy*-plane. Each of the models considered in this approach have long grains that measure 4.5*mm* in width. Analogous to T-L and L-T experiments, several explicitly modeled SC grains are aligned in the *x* and *y*-direction, respectively. A pure transformation referenced from the *y*-axis was applied to each of the grain lattices. Since the material is cubic, the maximum tilt boundary misorientation achievable in the Euler space is *p/4*. Aside from lattice orientation, SC grains are otherwise identical. Twist misorientation angles were not considered.

The C^*-integral can be calculated along particular contours enclosing the crack tip; however, Moran and Shih [7] restated this as an area integral to improve efficiency when using FEA results

$$C^* = \int_{A_\Gamma} \left(s_{ij} \frac{\partial u_j}{\partial x_1} - W^* d_{1i} \right) \frac{\partial q_1}{\partial x_i} dA_\Gamma \tag{7}$$

where q_1 is a dimensionless pyramidal weight function over the area, A_G. The so-called Equivalent Domain/Area Integral method is versatile and accurate over a variety of time-dependent material regimes. Asymptotic fields within A_G were used to evaluate Eq. (7).

4 RESULTS

The crack tip behavior of models with *homogenized grains* depends on the DS direction, b. Symmetric asymptotic fields are only realized when the material is symmetric about the crack plane (i.e., either parallel or perpendicular to the load axis). This phenomenon is demonstrated by the angular distribution of the effective stresses surrounding the crack. When the crystallographic orientation of the material is nearly geometrically symmetric about the crack tip (i.e., b=0° or 90°), the asymptotic fields are insensitive to small rotations of the material of ±15° relative to the loading axis. Conversely, for cases when the DS axis is between 30° and 60° relative to the loading axis, the crack tip fields exhibit marked sensitivity to small rotations since the creep

compliant axis of the material is nearly aligned with the direction where crack tip stresses are maximum.

Transversely isotropic cases with ratios accounting for higher (H=0.41) or lower (H=0.25, 0.13, or 0.05) creep compliance than the baseline case (H=0.35) were also explored for lattice orientation dependence. For each of the aforementioned cases, the extensive steady state fracture parameter C^* is shown for various lattice orientations in Fig. 2. Each value has been normalized by the C^*-integral for the isotropic case, $C^*_{H=0.5}$. Since C^* is generally proportional to crack growth rates, the crack growth rate for this material should be minimized when propagating along the direction transverse to the DS axis. If crack propagation is permitted, the accuracy of the near tip field response can be validated if the simulated d-curves exhibit resemblance with those recorded from experiments. Figure 3 illustrates these load line curves for both the *homogenized* and *explicit* modeling approaches. For the former case, the magnitude of crack tip deformation allows for good correlation with L-T data; in the latter case, T-L curves overlap with experimental data regardless of tilt misorientation between SC grains.

At the simulated temperature and K_I level, the material displayed creep-ductile behavior. The elastic contribution to the overall deflection rate, from Eq. (1), is negligible, and creep zone expansion exceeded the crack propagation rate. Effective 2% strain creep zones in explicitly modeled SCs oriented in the L-T and T-L directions are shown in Fig. 4. For each case the creep zone shape is influenced by GB location. In this regard, GB interfaces either shield or enhance inelastic deformation, thus making grain width and misorientation key microstructural factors controlling the crack tip response. Additionally, since the interface between adjacent grains influences the crack tip fields, self-similitude is only realized when the SCs are aligned (w=0°).

5 CONCLUSIONS

Crack tip behavior of a DS Ni-base superalloy has been studied. Simulations incorporated an elasto-creep relation with constants optimized according to experimental data. This constitutive model was used to simulate anisotropic deformation occurring in fracture specimen consisting of a generic DS Ni-base turbine blade material at 871°C. Fracture specimens designed to exhibit either stationary or growing crack tip behavior were used to determine the HRR-type fields. Models with *homogenized microstructures* produced asymptotic fields that are sensitive to orientation of the DS axis relative to the loading direction. These asymptotic stress, strain, and displacement fields were post-processed to determine C^*. Other cases, in which the microstructures consisted of *explicitly modeled long SC grains*, lead to crack tip fields that were generally independent of GB misorientation, but dependent on the solidification direction. These phenomena were reflected in crack tip response measures such as the load line deflection.

References

1. Nazmy, M. Y., and Wuthrich, C., *Materials Science and Engineering* **61**, 119-125, 1983.
2. Gardner, B., Saxena, A., and Qu, J., *in* "International Conference on Fracture (ICF10)," Elsevier Science, Honolulu, HI, 2001.
3. Ibanez, A. R., PhD Thesis, Georgia Institute of Technology, Atlanta, GA, 2003.
4. Landes, J. D., and Begley, J. A., *in* "Fracture Analysis, ASTM STP 590," ASTM, Philadelphia, 1976.
5. Nikbin, K. M., Webster, G. A., and Turner, C. E., *in* "Fracture Analysis, ASTM STP 601," ASTM, Philadelphia, 1976.
6. Riedel, H., and Rice, J. R., *in* "Fracture Mechanics, ASTM STP 700," ASTM, Philadelphia, 1980.
7. Moran, B., and Shih, C. F., *Engineering Fracture Mechanics* **27**, 615-642, 1987.